AIP Advances

Ion-gated transistors based on porous and compact TiO_2 films: Effect of Li ions in the gating medium

Cite as: AIP Advances **10**, 065314 (2020); https://doi.org/10.1063/5.0009984
Submitted: 05 April 2020 . Accepted: 21 May 2020 . Published Online: 12 June 2020

Arunprabaharan Subramanian, Ben George, Sanyasi Rao Bobbara, Irina Valitova, Irene Ruggeri, Francesca Borghi, Alessandro Podestà, Paolo Milani, Francesca Soavi, Clara Santato, and Fabio Cicoira

Ion-gated transistors based on porous and compact TiO_2 films: Effect of Li ions in the gating medium

Cite as: AIP Advances 10, 065314 (2020); doi: 10.1063/5.0009984
Submitted: 5 April 2020 • Accepted: 21 May 2020 •
Published Online: 12 June 2020

Arunprabaharan Subramanian,[1] Ben George,[1] Sanyasi Rao Bobbara,[1] Irina Valitova,[1] Irene Ruggeri,[1,2] Francesca Borghi,[3] Alessandro Podestà,[3] Paolo Milani,[3] Francesca Soavi,[2] Clara Santato,[4] and Fabio Cicoira[1,a)]

AFFILIATIONS

[1]Department of Chemical Engineering, Polytechnique Montréal, Montréal, Quebec H3T 1J4, Canada
[2]Dipartimento di Chimica "Giacomo Ciamician", Università di Bologna, Via Selmi 2, Bologna 40126, Italy
[3]CIMaINa and Dipartimento di Fisica "Aldo Pontremoli", Università degli Studi di Milano, Via Celoria 16, Milano 20133, Italy
[4]Department of Engineering Physics, Polytechnique Montréal, Montréal, Quebec H3T 1J4, Canada

[a)]**Author to whom correspondence should be addressed:** fabio.cicoira@polymtl.ca

ABSTRACT

Ion-gated transistors (IGTs) are attractive for chemo- and bio-sensing, wearable electronics, and bioelectronics, because of their ability to act as ion/electron converters and their low operating voltages (e.g., below 1 V). Metal oxides are of special interest as transistor channel materials in IGTs due to their high mobility, chemical stability, and the ease of processing in air at relatively low temperatures (<350 °C). Titanium dioxide is an abundant material that can be used as a channel material in *n*-type IGTs. In this work, we investigate the role of the morphology of the TiO_2 channel (porous vs compact films) and the size of the cations in the gating media ([EMIM][TFSI] and [Li][TFSI] dissolved in [EMIM][TFSI]) to study their role on the electrical characteristics of IGTs. We found that both the film morphology and the type of gating medium highly affect the electrical response of the devices.

Metal oxide semiconductors are exploited in a variety of applications, such as sensing, energy conversion and storage, and display technologies.[1–4] They are widely studied as active channel materials for thin-film transistors (TFTs) and ion-gated transistors (IGTs) due to their abundance, chemical stability, transparency, and the ease of processing at low temperatures under ambient conditions.[5,6] Amorphous indium–gallium–zinc-oxide (a-IGZO) is currently used in *n*-type TFT backplanes of flat panel and organic light-emitting diode (OLED) displays, due to its high electrical conductivity, film uniformity, and transparency, as well as its mechanical and chemical stability.[3,7–11] Indium-based oxides also show excellent performance as channel materials for IGTs (charge carrier mobility up to ~120 $cm^2\ V^{-1}\ s^{-1}$).[12] However, as the availability of indium in the earth's crust is limited, there is an increasing interest in indium-free metal oxides, such as ZnO, SnO_2, Cu_xO, NiO, and TiO_2, both for TFTs and IGTs.[5,13–28] Among indium-free metal oxides, TiO_2 (*n*-type) is sought for its availability, cost-effective processability, high chemical stability, and biocompatibility.[29,30] Our groups reported on TiO_2-based IGTs using 1-ethyl-3-methylimidazolium bis(trifluoromethylsulfonyl)imide ([EMIM][TFSI]) as the gating medium and found that the patterning of the channel leads to enhanced transistor performance.[19]

IGTs use ion-gating media, such as aqueous saline solutions, polymer electrolytes, ionic liquids, and ion gels. A high specific capacitance (~10–100 $\mu F/cm^2$), which permits operation at low voltages (<2 V), is achieved by the formation of a thin electrical double layer at the semiconductor/gating medium interface. Besides pure electrostatic or electrochemical doping, different mechanisms have been considered to describe the operation of IGTs, such as interface-confined electrochemical doping.[6,21,31–37]

In this work, we explored IGTs based on TiO_2 active layers deposited using thermal evaporation to produce compact films, and solution casting to produce porous films. Transistors based on compact films show electron mobilities about two orders of magnitude higher than those based on porous ones. In order to gain further insight into the doping mechanism, we employed two gating media: [EMIM][TFSI] and lithium bis(trifluoromethanesulfonyl)imide ([Li][TFSI]) dissolved in [EMIM][TFSI]. The characteristics of transistors based on compact and porous films depend on the gating media, which points to different working mechanisms. While $[EMIM]^+$ ions (ionic radius ~ 3.5 Å) are expected to dope TiO_2 by electrostatic and interface-confined electrochemical doping,[19] $[Li]^+$ ions, having a small radius (~0.7 Å), are expected to dope TiO_2 electrochemically via lattice intercalation.[38–40]

Thermal (e-beam) evaporation was carried out at a deposition rate of 0.7 Å/s and a pressure of 3×10^{-5} Torr using a Thermionics e-beam evaporator. Solution processed TiO_2 films were obtained by drop casting a suspension containing 2 g of TiO_2 (a mixture of rutile and anatase in xylene, MilliporeSigma, No. 700339) and 0.4 g of polyvinylidene fluoride (PVDF, MilliporeSigma) binder in 20 ml of dimethylformamide (DMF, Caledon Laboratory Chemicals, purity 98.5%). The suspension was mixed in a planetary mixer (Thinky ARM-310) for 30 min at 2000 rpm and then filtered through a 0.2 μm nylon filter. Finally, it was drop cast on the substrates that were first heated at 60 °C for 30 min to remove excess solvent, and subsequently annealed at 450 °C in a tube furnace for 1 h in ambient air.[19] The thicknesses of the films, measured using a profilometer (Dektak 150) were ~60 nm for the evaporated films and ~3 μm for the drop-cast films. A high thickness was required for the drop-cast films in order to achieve a complete coverage of the portion of the substrate containing the devices (Fig. S1).

The scanning electron microscopy (SEM) analysis was performed using JEOL FEG-SEM, JSM 7600F. The x-ray diffraction (XRD) study was performed with a Bruker D8 diffractometer using a CuKα beam, at every $2\theta = 0.01°$. The atomic force microscopy (AFM) study was performed using a Multimode Nanoscope (Bruker) in tapping mode, in air, using Bruker NCHV probes with the resonance frequency between 270 KHz and 400 KHz, k = 40 N/m, and a nominal tip radius of 8 nm.

Ion-gated transistors were fabricated according to a procedure described in previous publications.[19,20] The TiO_2 films were deposited, as described above, on SiO_2/Si substrates pre-patterned with Ti/Au (5 nm/40 nm) source–drain electrodes (W/L = 4000 μm/10 μm) by vacuum sublimation and drop casting. As gating media, we used 1-ethyl-3-methylimidazolium bis(trifluoromethylsulfonyl)imide [EMIM][TFSI] (IoLiTec GmbH) and a mixture of 10 ml [EMIM][TFSI] and 0.86 g [Li][TFSI] (MilliporeSigma), both saturating a Durapore® PVDF 0.22 μm membrane. Activated carbon (PICACTIF SUPERCAP BP10) on carbon paper (Spectracarb 2050) was used as the gate electrode. The high surface area (~1000 $m^2\ g^{-1}$ to 2000 $m^2\ g^{-1}$) of this electrode is amenable to high current modulation, while its inertness toward undesired electrochemical reactions is advantageous for device stability.[19,41]

Transistor characteristics were measured in a N_2-purged glove box (O_2 and H_2O < 3 ppm) with a semiconductor parameter analyzer (Agilent B1500A). We prepared four types of transistors, based on evaporated and solution-processed TiO_2 channels and two different gating media, i.e., [EMIM][TFSI] and 0.3M [Li][TFSI] in [EMIM][TFSI]. The transistor characterization was performed at a sweep rate of 50 mV/s. Cyclic voltammetry (CV) was performed using a Princeton Applied Research VERSASTAT 4 potentiostat (see Fig. S2 for the device configuration during cyclic voltammetry). Device characterization was performed in the following order: cyclic voltammetry (three cycles were performed, the third cycle is reported), output characteristics, transfer characteristics in the linear regime (three cycles were performed, the second cycle is reported), and transfer characteristics in the saturation regime (three cycles were performed, the second cycle is reported).

SEM and AFM images reveal that the evaporated films are compact, with a root mean square (rms) roughness of 1.0 ± 0.1 nm [Fig. 1(a) and Figs. S3a and S3b], while the solution-processed ones are porous with a rms roughness of 117 ± 5 nm [Fig. 1(b) and Figs. S3c and S3d]. According to the XRD patterns, the TiO_2 evaporated films primarily consist of the anatase phase [Fig. 1(c)], while the solution-processed ones consist of a mixture of anatase and rutile phases [Fig. 1(d)].[19]

Figure 2 shows the output and transfer characteristics of evaporated TiO_2 transistors gated with [EMIM][TFSI] [Figs. 2(a)–2(c)] and [Li][TFSI] + [EMIM][TFSI] [Figs. 2(d)–2(f)]. All the devices show *n*-type behavior and function below 1.5 V. Gating with [Li][TFSI] + [EMIM][TFSI] produces an increase in the transistor current of about a factor of 2. The transfer curves [Figs. 2(b) and 2(e)] show hysteresis indicating slow ion transport (see Fig. S4 for the hysteresis loop area calculation and Table S1 for the values of hysteresis loop area of evaporated TiO_2 IGTs).[21,42] The threshold voltages, extracted from the linear transfer characteristics, are in the range of 0.4 V–0.5 V for both gating media (Table S2). The saturation (V_{ds} = 1 V) transfer characteristics [Figs. 2(c) and 2(f)] show that the ON/OFF ratios are rather low (Table S2) due to high OFF currents (about 10^{-4}–10^{-3} A), which might be attributed to the higher intrinsic conductivity of the evaporated TiO_2 films.

Figure 3 shows the output and transfer characteristics of solution-processed TiO_2 IGTs using [EMIM][TFSI] [Figs. 3(a)–3(c)] and [Li][TFSI] + [EMIM][TFSI] [Figs. 3(d)–3(f)] acquired at a sweep rate of 50 mV/s. Solution-processed TiO_2 IGTs show a lower drain current than the evaporated ones. Both output and transfer characteristics (Fig. 3) show that gating with [Li][TFSI] + [EMIM][TFSI] dramatically affects transistor characteristics, producing an increase in the transistor saturation current of about a factor of 20. The drain current saturation is clearly observed for the solution processed devices. Transfer characteristics in the linear regime [Figs. 3(b) and 3(e)] show hysteresis for both gating media. The areas of the hysteresis loops in the [EMIM][TFSI] gated devices are smaller than those of the [Li][TFSI] + [EMIM][TFSI] gated devices, due to the lower drain current and the higher threshold voltage, especially for the solution processed devices (Table S3). The areas of the hysteresis loops in the evaporated devices are not affected by the gating media, and their values are similar to those of the [Li][TFSI] + [EMIM][TFSI] gated solution-processed devices (Tables S1 and S3). The threshold voltages extracted from the linear transfer characteristics were 1.3 V for the devices gated with [EMIM][TFSI] and 0.9 V for those gated with [Li] [TFSI] + [EMIM] [TFSI] (Table S4). The ON/OFF ratios, extracted from

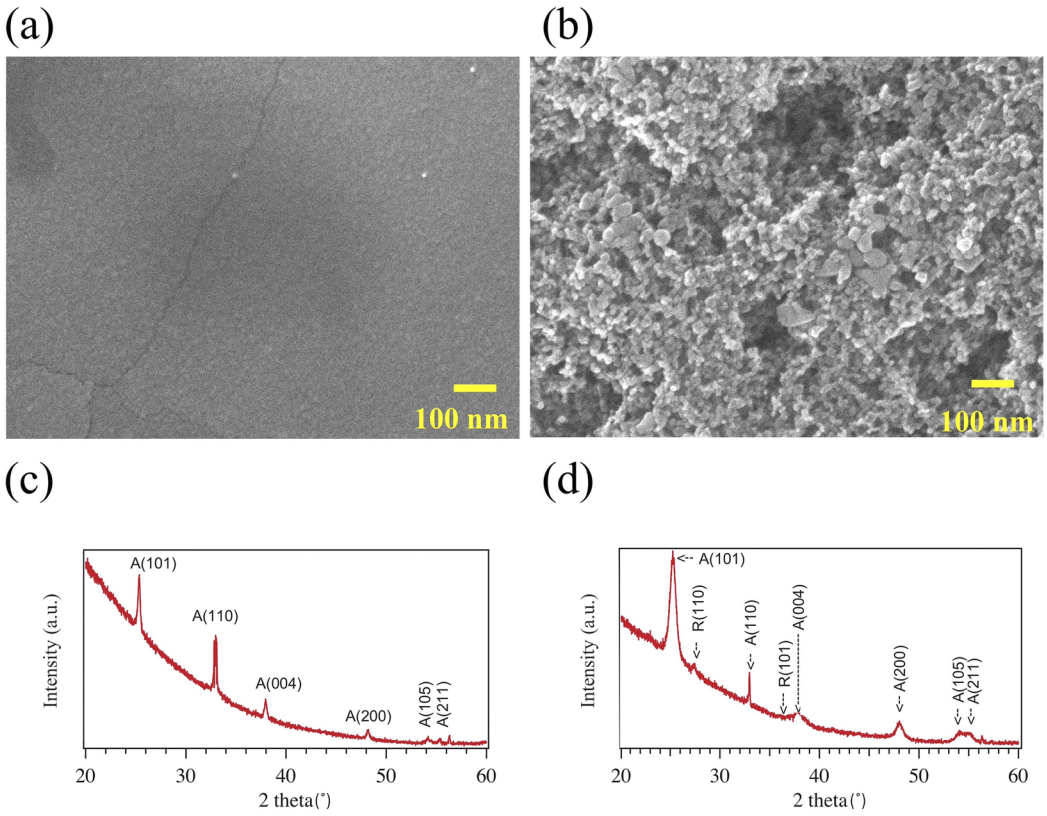

FIG. 1. SEM images of (a) evaporated and (b) solution-processed TiO_2 films. XRD patterns of the (c) evaporated and (d) solution-processed[19] TiO_2 films. A and R indicate the peaks of the anatase [Joint Committee on Powder Diffraction Standards (JCPDS) card number: 01-089-4203] and rutile (JCPDS card number: 01-083-2242) phases of TiO_2. Figure (d) is reproduced with permission from Valitova *et al.*, ACS Appl. Mater. Interfaces **8**(23), 14855 (2016). Copyright 2016 American Chemical Society.

the saturation regime of transfer characteristics [Figs. 3(c) and 3(f)] were 40 for the devices gated with [EMIM] [TFSI] and 10^3 for the devices gated with [Li] [TFSI] + [EMIM] [TFSI] (Table S4).

The effect of the gating medium on the transistor current can be explained by a change in the doping mechanism; while the large $[EMIM]^+$ ions likely lead to a combination of electrostatic and interface-confined electrochemical doping,[19,21] the smaller $[Li]^+$ ions ($r_{EMIM}{}^+/r_{Li}{}^+ \sim 5$) might lead to electrochemical doping via the intercalation of Li^+ ions in the TiO_2 lattice.[38,39] The number of Li intercalation events is favored by the porous morphology of the solution processed films, which explains the much larger difference in the saturation current and ON/OFF ratio with respect to $[EMIM]^+$ gating. Moreover, the small size of Li^+ ions (~0.7 Å)[38] also facilitates a higher packing density at the gating media/TiO_2 interface, which might lead to more efficient electrostatic and interface-confined electrochemical doping.

The charge carrier mobility was extracted from the transfer characteristics in the linear regime according to the formula $\mu_{lin} = \frac{L I_{d,lin}}{W e n V_d}$, where L indicates the interelectrode distance (10 μm), W the electrode width (4000 μm), V_d the drain–source voltage (0.1 V), n the charge carrier density, e the elementary charge (1.6×10^{-19} C), and $I_{d,lin}$ the drain–source current at 1.5 V.[19] The charge carrier density is calculated from the linear transfer characteristics, using the formula $n = \frac{Q}{eA} = \frac{\int I_g dV_g}{r_v e A}$, where Q is the doping charge, I_g is the gate–source current in the forward scan [Figs. 2(b), 2(e), 3(b), and 3(e)], r_v is the sweep rate of the gate voltage, and A is the surface area of the semiconductor in contact with the membrane soaked with the gating media (in our case 0.36 ± 0.04 cm^2).[19] For the porous films, we also calculated the mobility using the surface area of the same region measured from Brunauer–Emmett–Teller (BET) analysis (see the supplementary material).[19,42] The calculated charge carrier densities and mobilities are summarized in Tables S4 and S5. For evaporated TiO_2 IGTs, a charge carrier mobility of ~0.5 cm^2/V s was extracted for both gating media (Table S2). The obtained mobility value is comparable with values reported in the previous articles based on metal oxide TFTs and IGTs.[17–19,25,27,43–46] Solution-processed TiO_2 IGTs showed a lower mobility with a significant dependence on the gating media. For the devices gated with [EMIM][TFSI], we obtained a charge carrier density of ~2×10^{15} cm^{-2} leading to a charge carrier mobility of 5×10^{-4} cm^2 V^{-1} s^{-1}, while for those gated with [Li][TFSI] + [EMIM][TFSI], we obtained a charge carrier density of ~6×10^{15} cm^{-2} leading to a charge carrier mobility of ~4×10^{-3} cm^2 V^{-1} s^{-1}. The solution-processed

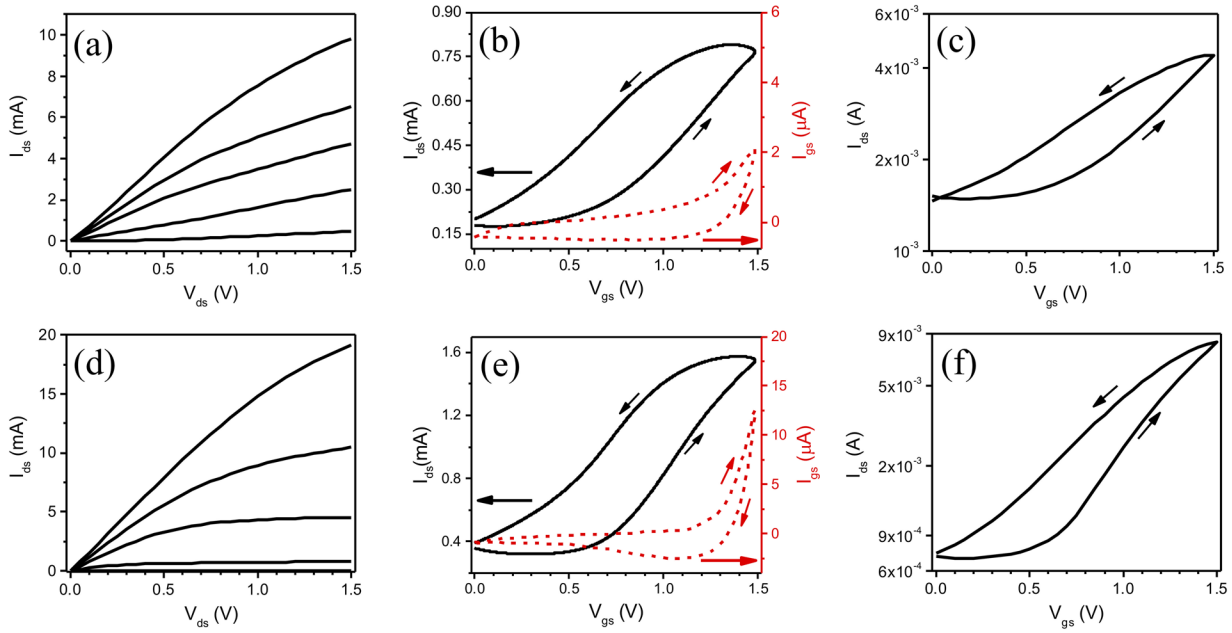

FIG. 2. Output and transfer characteristics in the linear and saturation regimes of transistors based on the evaporated TiO_2 films (~60 nm thick) gated with [EMIM][TFSI] (a)–(c), and [Li][TFSI] + [EMIM][TFSI] (d)–(f) measured with a sweep rate of 50 mV/s. The output characteristics were acquired at V_{gs} = 0 V, 1 V, 1.2 V, 1.3 V, and 1.5 V (a) and (d) and the transfer characteristics at $V_{ds,lin}$ = 100 mV (b) and (e) and at $V_{ds,sat}$ = 1 V (c) and (f). The transfer characteristics in the saturation (c) and (f) regime are represented on a logarithmic drain–source current scale. The dashed lines in the linear transfer characteristics (b) and (e) indicate the gate–source current of the devices.

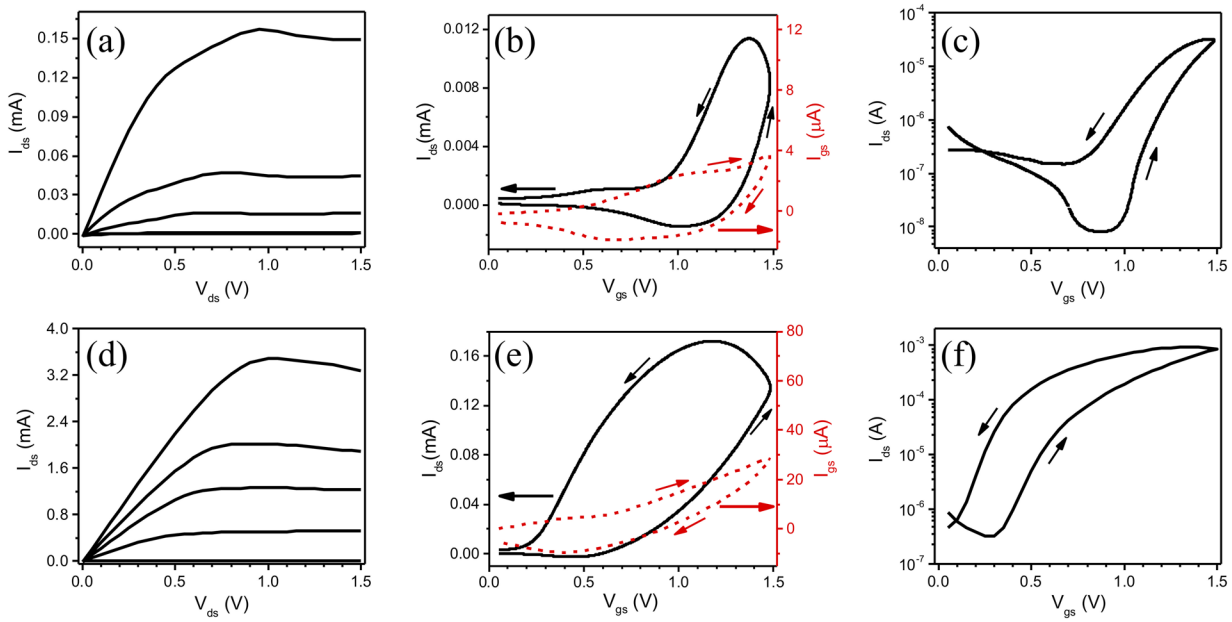

FIG. 3. Output and transfer characteristics in the linear and saturation regimes of transistors based on the solution-processed TiO_2 films (~3 μm thick) gated with [EMIM][TFSI] (a)–(c), and [Li][TFSI] + [EMIM][TFSI] (d)–(f) measured with a sweep rate of 50 mV/s. The output characteristics were acquired at V_{gs} = 0 V, 1 V, 1.2 V, 1.3 V, and 1.5 V (a) and (d) and the transfer characteristics at $V_{ds,linear}$ = 100 mV (b) and (e) and at $V_{ds,saturation}$ = 1 V (c) and (f). The transfer characteristics in the saturation (c) and (f) regime are represented on a logarithmic drain–source current scale. The dashed lines in the linear transfer characteristics (b) and (e) indicate the gate–source current of the devices.

devices show a large spread in the charge carrier density and mobility values, likely due to the less reproducible film deposition technique.[47]

Figure 4 shows the cyclic voltammetry (CV) of the evaporated and solution-processed TiO_2 based IGTs with [EMIM][TFSI] and [Li][TFSI] + [EMIM][TFSI], performed in a two-electrode configuration, with the TiO_2 channel acting as the working electrode and the activated carbon gate (specific capacitance of ~100 F/g) acting simultaneously as the counter and quasi-reference electrode.[41]

The currents obtained with solution-processed TiO_2 are higher than those measured with the evaporated TiO_2 films due to their higher thickness.

The cyclic voltammetries show wide cathodic and anodic waves related to the reversible reduction–oxidation process of TiO_2. The cathodic signal represents the n-doping of TiO_2 and the anodic one represents the dedoping process. For the evaporated films, redox processes are evident below −0.7 V for both gating media [Figs. 4(a) and 4(b)]. The CVs also indicate an irreversible cathodic process occurring below −1.3 V, which is more evident for [Li][TFSI] + [EMIM][TFSI] gating. For solution-processed TiO_2, the absence of defined peaks is indicative of the pseudocapacitive behavior at potentials lower than −0.7 V for the devices gated with [EMIM][TFSI] [Fig. 4(c)] and lower than −0.5 V for the devices gated with [Li][TFSI] + [EMIM][TFSI] [Fig. 4(d)].[19] In the case of solution-processed TiO_2 gated with [Li][TFSI] + [EMIM][TFSI], additional cathodic and anodic peaks are observed at −0.6 V and −0.25 V [Fig. 4(d)].

From the area encompassed by the CV loop, it can be discerned that the solution-processed TiO_2 based IGTs [Figs. 4(c) and 4(d)] have higher charge storage capacity than their evaporated TiO_2 counterparts [Figs. 4(a) and 4(b)]. Pseudocapacitance values of all the devices, calculated by the slope of doping charge vs voltage plots, are summarized in Tables S6 and S7 (for the porous solution-processed TiO_2 films, we also included values calculated using the BET surface area). The porous films have higher pseudocapacitance than the compact films; hence, the former can store more charge. All the devices show a high pseudocapacitance at low sweep rates. $[Li]^+$ based gating media lead to a higher pseudocapacitance than do the pure $[EMIM]^+$ based gating media.

In summary, we investigated the electrical and electrochemical properties of *n*-type IGTs based on evaporated (predominantly anatase) and solution-processed (mixture of rutile and anatase) polycrystalline TiO_2 films as channel materials, doped by [EMIM][TFSI] and [Li][TFSI] dissolved in [EMIM][TFSI].[48] The transistor characteristics of the evaporated films are not significantly affected by the presence of Li^+ in the gating medium. For the solution-processed films, the presence of Li^+ in the gating medium leads to a significant increase in the electron mobility. We hypothesize that the presence of Li^+ facilitates charge transport at grain boundaries in the solution-processed films. The evaporated TiO_2 films show a higher mobility of 0.5 $cm^2\ V^{-1}\ s^{-1}$ compared to the solution-processed films. The charge carrier density is not dramatically affected by the presence of Li^+ in [EMIM][TSFI], as we could have expected considering the different ion size

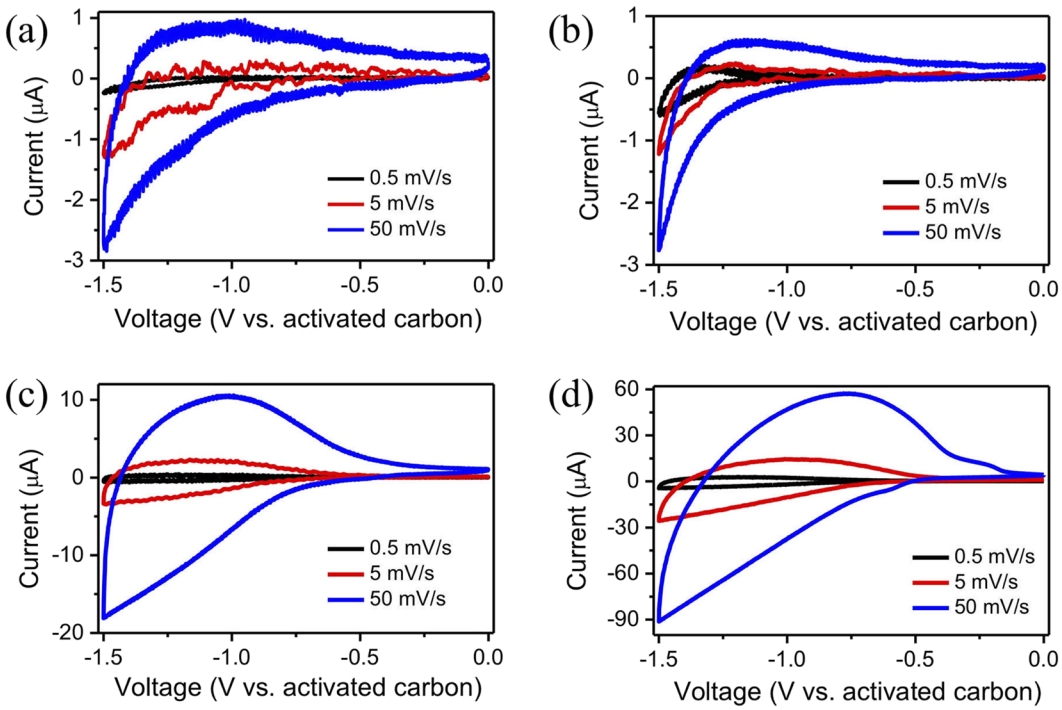

FIG. 4. Cyclic voltammetry of transistors based on the evaporated TiO_2 films gated with [EMIM][TFSI] (a) and [Li][TFSI] + [EMIM][TFSI] (b), and the solution processed TiO_2 films gated with [EMIM][TFSI] (c) and [Li][TFSI] + [EMIM][TFSI] (d), at 0.5 mV/s, 5 mV/s, and 50 mV/s, respectively.

(~0.7 Å for Li^+ vs 3.5 Å for $[EMIM]^+$). This points to the complex arrangements of the ions in the electrical double layer. Work is in progress to shed light on such complexity (originated from the number of ionic interactions, from electrostatic to van der Waals) by atomic force microscopy force–distance profiling performed in highly viscous ionic liquids.[49]

See the supplementary material for the schematic representation of the coverage of the TiO_2 film on the substrate, device configuration during the electrical and electrochemical characterizations, AFM images of the TiO_2 films, explanation of the hysteresis loop area calculations, values of hysteresis loop area, charge carrier density, mobility, ON/OFF ratio, threshold voltage of IGTs, and the pseudocapacitance values of the TiO_2 films.

The authors are grateful to Yves Drolet for technical assistance. Funding for this project was provided by NSERC (Discovery grants, F.C. and C.S.) and the Québec Ministry of Economy Science and Innovation (Project No. PSR-SIIRI-810). I.V. and A.S. are grateful to FRQNT for financial support through a doctoral scholarship, A.S. is grateful to the Trottier Energy Institute for a doctoral scholarship, and B.G. is grateful to FRQNT for a Master's scholarship. F.S. acknowledges financial support from Alma Mater Studiorum Università di Bologna (Researcher Mobility Program, Italian-Canadian cooperation agreement). This work was supported by CMC Microsystems through the MNT program. This work also benefited from the financial support of FRQNT through a grant awarded to RQMP.

DATA AVAILABILITY

The data that support the findings of this study are available from the corresponding author upon reasonable request.

REFERENCES

[1] E. Fortunato, P. Barquinha, and R. Martins, Adv. Mater. **24**, 2945 (2012).
[2] X. Yu, T. J. Marks, and A. Facchetti, Nat. Mater. **15**, 383 (2016).
[3] W. Xu, H. Li, J.-B. Xu, and L. Wang, ACS Appl. Mater. Interfaces **10**, 25878 (2018).
[4] T. Tachikawa and T. Majima, NPG Asia Mater. **6**, e100 (2014).
[5] J. W. Park, B. H. Kang, and H. J. Kim, Adv. Funct. Mater. **30**, 1904632 (2019).
[6] C. Leighton, Nat. Mater. **18**, 13 (2019).
[7] J. Sheng, T. Hong, H.-M. Lee, K. Kim, M. Sasase, J. Kim, H. Hosono, and J.-S. Park, ACS Appl. Mater. Interfaces **11**, 40300 (2019).
[8] G. Cantarella, C. Vogt, R. Hopf, N. Münzenrieder, P. Andrianakis, L. Petti, A. Daus, S. Knobelspies, L. Büthe, and G. Tröster, ACS Appl. Mater. Interfaces **9**, 28750 (2017).
[9] G. Cantarella, N. Münzenrieder, L. Petti, C. Vogt, L. Büthe, G. A. Salvatore, A. Daus, and G. Tröster, IEEE Electron Device Lett. **36**, 781 (2015).
[10] G. Cantarella, V. Costanza, A. Ferrero, R. Hopf, C. Vogt, M. Varga, L. Petti, N. Münzenrieder, L. Büthe, and G. Salvatore, Adv. Funct. Mater. **28**, 1705132 (2018).
[11] K. Nomura, H. Ohta, A. Takagi, T. Kamiya, M. Hirano, and H. Hosono, Nature **432**, 488 (2004).
[12] S. K. Garlapati, N. Mishra, S. Dehm, R. Hahn, R. Kruk, H. Hahn, and S. Dasgupta, ACS Appl. Mater. Interfaces **5**, 11498 (2013).
[13] C. W. Shih and A. Chin, Sci. Rep. **7**, 1147 (2017).
[14] C. W. Shih, A. Chin, C. F. Lu, and W. F. Su, Sci. Rep. **6**, 19023 (2016).
[15] S. Y. Kim, C. H. Ahn, J. H. Lee, Y. H. Kwon, S. Hwang, J. Y. Lee, and H. K. Cho, ACS Appl. Mater. Interfaces **5**, 2417 (2013).
[16] A. Liu, H. Zhu, Z. Guo, Y. Meng, G. Liu, E. Fortunato, R. Martins, and F. Shan, Adv. Mater. **29**, 1701599 (2017).
[17] W. S. Shih, S. J. Young, L. W. Ji, W. Water, and H. W. Shiu, J. Electrochem. Soc. **158**, H609 (2011).
[18] F. Zare Bidoky, B. Tang, R. Ma, K. S. Jochem, W. J. Hyun, D. Song, S. J. Koester, T. P. Lodge, and C. D. Frisbie, Adv. Funct. Mater. **30**, 1902028 (2019).
[19] I. Valitova, P. Kumar, X. Meng, F. Soavi, C. Santato, and F. Cicoira, ACS Appl. Mater. Interfaces **8**, 14855 (2016).
[20] I. Valitova, M. M. Natile, F. Soavi, C. Santato, and F. Cicoira, ACS Appl. Mater. Interfaces **9**, 37013 (2017).
[21] X. Meng, F. Quenneville, F. Venne, E. Di Mauro, D. Işık, M. Barbosa, Y. Drolet, M. M. Natile, D. Rochefort, and F. Soavi, J. Phys. Chem. C **119**, 21732 (2015).
[22] R. Horita, K. Ohtani, T. Kai, Y. Murao, H. Nishida, T. Toya, K. Seo, M. Sakai, and T. Okuda, Jpn. J. Appl. Phys., Part 1 **52**, 115803 (2013).
[23] T. D. Schladt, T. Graf, N. B. Aetukuri, M. Li, A. Fantini, X. Jiang, M. G. Samant, and S. S. P. Parkin, ACS Nano **7**, 8074 (2013).
[24] Y.-L. Han, Z.-Z. Luo, C.-J. Li, S.-C. Shen, G.-L. Qu, C.-M. Xiong, R.-F. Dou, L. He, and J.-C. Nie, Phys. Rev. B **90**, 205107 (2014).
[25] W.-C. Peng, Y.-C. Chen, J.-L. He, S.-L. Ou, R.-H. Horng, and D.-S. Wuu, Sci. Rep. **8**, 9255 (2018).
[26] S. M. Chung, J.-H. Shin, C.-H. Hong, and W.-S. Cheong, J. Nanosci. Nanotechnol. **12**, 5440 (2012).
[27] H. Choi, J. Shin, and C. Shin, ECS J. Solid State Sci. Technol. **6**, P379 (2017).
[28] H. Y. Chong and T. W. Kim, J. Electron. Mater. **42**, 398 (2013).
[29] J. Tian, Z. Zhao, A. Kumar, R. I. Boughton, and H. Liu, Chem. Soc. Rev. **43**, 6920 (2014).
[30] A. Weir, P. Westerhoff, L. Fabricius, K. Hristovski, and N. Von Goetz, Environ. Sci. Technol. **46**, 2242 (2012).
[31] S. Z. Bisri, S. Shimizu, M. Nakano, and Y. Iwasa, Adv. Mater. **29**, 1607054 (2017).
[32] S. H. Kim, K. Hong, W. Xie, K. H. Lee, S. Zhang, T. P. Lodge, and C. D. Frisbie, Adv. Mater. **25**, 1822 (2013).
[33] T. Fujimoto and K. Awaga, Phys. Chem. Chem. Phys. **15**, 8983 (2013).
[34] H. Du, X. Lin, Z. Xu, and D. Chu, J. Mater. Sci. **50**, 5641 (2015).
[35] H. Yuan, H. Shimotani, J. Ye, S. Yoon, H. Aliah, A. Tsukazaki, M. Kawasaki, and Y. Iwasa, J. Am. Chem. Soc. **132**, 18402 (2010).
[36] M. Barbosa, F. M. Oliveira, X. Meng, F. Soavi, C. Santato, and M. Orlandi, J. Mater. Chem. C **6**, 1980 (2018).
[37] J. D. Yuen, A. S. Dhoot, E. B. Namdas, N. E. Coates, M. Heeney, I. McCulloch, D. Moses, and A. J. Heeger, J. Am. Chem. Soc. **129**, 14367 (2007).
[38] S. Moitzheim, S. De Gendt, and P. M. Vereecken, J. Electrochem. Soc. **166**, A1 (2019).
[39] H. Lindström, S. Södergren, A. Solbrand, H. Rensmo, J. Hjelm, A. Hagfeldt, and S.-E. Lindquist, J. Phys. Chem. B **101**, 7717 (1997).
[40] C. G. Granqvist, *Handbook of Inorganic Electrochromic Materials*, 1st ed. (Elsevier, 1995).
[41] J. Sayago, F. Soavi, Y. Sivalingam, F. Cicoira, and C. Santato, J. Mater. Chem. C **2**, 5690 (2014).
[42] G. V. D. O. Silva, A. Subramanian, X. Meng, S. Zhang, M. S. Barbosa, B. Baloukas, D. Chartrand, J. C. Gonzáles, M. O. Orlandi, and F. Soavi, J. Phys. D: Appl. Phys. **52**, 305102 (2019).
[43] M. Katayama, S. Ikesaka, J. Kuwano, H. Koinuma, and Y. Matsumoto, Appl. Phys. Lett. **92**, 132107 (2008).
[44] J.-W. Park and S. Yoo, IEEE Electron Device Lett. **29**, 724 (2008).
[45] G. Oike, T. Yajima, T. Nishimura, K. Nagashio, and A. Toriumi, in *IEEE International Electron Devices Meeting* (IEEE, 2013), p. 300.
[46] K.-H. Choi and H.-K. Kim, Electrochem. Solid State Lett. **14**, H314 (2011).
[47] M. Eslamian and F. Zabihi, Nanoscale Res. Lett. **10**, 462 (2015).
[48] A. Wahl and J. Augustynski, J. Phys. Chem. B **102**, 7820 (1998).
[49] M. Schwellberger Barbosa, N. Balke, W.-Y. Tsai, C. Santato, and M. O. Orlandi, J. Phys. Chem. Lett. **11**, 3257 (2020).